Analyzing Effects of Directionality and Random Heights in Drone-based mmWave Communication

Roman Kovalchukov, Dmitri Moltchanov, Andrey Samuylov, Aleksandr Ometov, *Member, IEEE*, Sergey Andreev, *Senior Member, IEEE*, Yevgeni Koucheryavy, *Senior Member, IEEE*, and Konstantin Samouylov

***Abstract*—Utilization of drones as aerial access points (AAPs) is a promising concept to enhance network coverage and area capacity promptly and on demand. The emerging millimeter-wave (mmWave) communication technology may in principle deliver higher data rates, thus making the use of AAPs more effective. By extending the conventional (planar) stochastic geometry considerations, we construct a novel three-dimensional model for drone-based mmWave communication that captures the high directionality of transmissions as well as the random heights of the communicating entities. Choosing signal-to-interference ratio (SIR) as our primary parameter of interest, we assess system performance with an emphasis on the impact of the 'vertical' dimension in aerial mmWave connectivity. We also demonstrate that accurate performance assessment is only possible with simplified models for certain ranges of input parameters.**

I. Introduction

Drones have recently received much attention by demonstrating the potential to be deployed as dedicated aerial access points (AAPs) for cellular users [1] or as mobile relay stations. The utilization of drones as AAPs may provide (i) on-demand capacity boost, (ii) prompt coverage by offering service in the so-called "blind spots", (iii) increased reliability and quality of service (QoS) by augmenting applications based on the use of licensed spectrum, and (iv) support for seamless session continuity as users move around [2], [3]. Provisional drone-based networks show a lot of promise to support future 5th generation (5G) services. Recently, both academia and industry studies have reported on the test trials of drone-assisted communication [4].

The use of drones as AAPs or relays brings novel unique challenges related to efficient spectrum management [5], [6]. Performance of drone-based communication from the perspective of service provisioning has been addressed already in the context of microwave 4th generation (4G) systems. The importance of accurate air-to-ground channel modeling was further stressed in [1]. In [7], the authors proposed a heuristic solution to enable drone-based AAPs and thus increase the spectral efficiency by 34% as well as the 5-percentile packet throughput by 50%. The effects of mobility, path loss, and elevation angle have additionally been taken into account. In [8], the authors elaborated a software-defined networking (SDN) solution for drone-based connectivity.

R. Kovalchukov, D. Moltchanov, A. Samuylov, A. Ometov, S. Andreev, and Y. Koucheryavy are with the Laboratory of Electronics and Communications Engineering, Tampere University of Technology, Tampere, Finland.

K. Samouylov is with Peoples' Friendship University of Russia (RUDN University), Moscow, Russia. and also with Federal Research Center "Computer Science and Control" of the Russian Academy of Sciences, Moscow, Russia.

Correspondence email: dmitri.moltchanov@tut.fi

Several studies addressed the question of integrating AAPs as part of the future cellular networks. With extensive simulations, the authors of [9] studied the application of drones as intermediate aerial nodes between the macro and the small cell tiers in a heterogeneous network (HetNet). They revealed that the proposed concept allows to improve the spectral efficiency by 38% and reduce the delay by up to 37.5% as compared to the terrestrial network baseline without drones. The coverage probability of mobile AAPs with underlaid device-to-device (D2D) communication capability has been addressed in [10], where the authors emphasized the importance of drone mobility in serving randomly scattered users. The study in [11] considered the optimal positioning strategies for drones.

One of the challenges in the emerging 5G millimeter-wave (mmWave) communication is the blockage of the line-of-sight (LoS) signal path between a user terminal and the mmWave access point (AP) [12]. To alleviate it, the concept of multi-connectivity has recently been proposed by 3GPP [13]. The use of drones as mmWave AAPs may thus bring decisive benefits to the network operators as both air-to-ground and backhaul links remain mostly in LoS conditions [14]. Shifting the focus to mmWave frequencies requires an extension of the conventional models by including specific features of inherently three-dimensional nature, such as *highly directional* antenna radiation patterns in both horizontal and vertical planes as well as *random heights* of communicating entities [14]. As most of past studies have been performed by assuming omnidirectional antennas, and hence rely on planar stochastic geometry, the effects of the 'vertical' dimension in drone-based mmWave communication have been addressed only marginally.

Extending the methods of stochastic geometry to the third dimension, we construct a novel mmWave AAP communication model by explicitly taking into account the random heights of drones and user equipment (UE) as well as the highly directional nature of mmWave links. We derive expressions for both the mean interference and the signal-to-interference ratio (SIR). Having these metrics at our disposal, we carry out a comprehensive numerical analysis that reveals the crucial effects in the considered characteristic scenario.

The following are the main contributions of this work:

- developing a methodology that allows to capture the effects of random heights of communicating entities and the directionality of antennas in interference and SIR modeling across the mmWave AAP communication scenarios;
- confirming that simpler models, which neglect the aforementioned effects, do not provide accurate assessment of

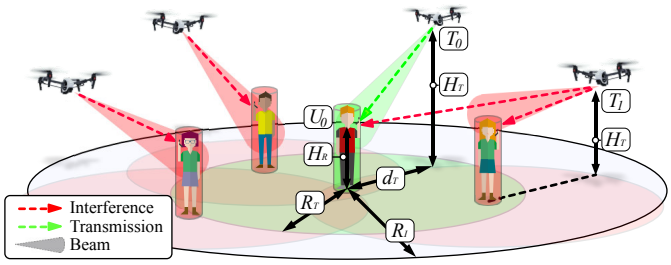

Fig. 1. Drone-based mmWave communication scenario in 3D.

SIR across the feasible range of system parameters;
- identifying the ranges of system parameters where simpler models provide sufficiently accurate approximations.

II. System Model and Assumptions

Our scenario of interest is displayed in Fig. 1. We concentrate on the downlink channel from the drone-based AAP to the UE on the ground. Assume that the locations of users are labeled as U_i, $i = 1, 2, \ldots$, and modeled by a Poisson point process in $\Re^2$ with the intensity of λ. The UEs are deployed at the height of H_R that is assumed to follow an exponential distribution with the parameter μ_R.

Each UE is associated with its corresponding serving AAP labeled as T_i. Positions of the AAPs are distributed uniformly within the circle of radius R_T centered at the UE of interest. The altitude distribution of drones is exponential with the parameter μ_T. Without loss of generality, all AAPs are assumed to utilize the same frequency, thus effectively acting as interferers for the tagged UE. Among the AAP-UE pairs, we randomly tag an arbitrary one as well as limit the area around such tagged UE to the radius of R_I. The interference created by the AAPs located outside of it is assumed to be negligible, i.e., lower than the noise floor. R_I is computed as a function of the propagation model, transmit power, and antenna directivity.

In the considered scenario, each UE benefiting from the AAP service is associated with a randomly chosen drone located not farther than a fixed planar distance away from it. In practice, this is implemented by listening on the air interface for the first beacon that can be correctly received/decoded and then associating with the AAP that had transmitted it.

Our selected path loss model is $L_P(r) = Cr^{-\gamma}$, where γ is the path loss exponent, while A is the factor accounting for the transmit power and antenna gains. Following [15], we assume a cone antenna model, where the radiation pattern is represented as a conical zone with the angle of α. This model is a simple abstraction assuming no side lobes as well as constant power at a certain distance from the AAP. One can determine C and γ by utilizing a propagation model for the frequency band of interest e.g., [16] for the spectrum range of $0.5 - 100$ GHz. Particularly, we have[1] $C = 10^{-2\log_{10}(\pi/\lambda)+0.49}$ and $\gamma = 2.1$.

[1]At the moment of writing, there are no standardized air-to-ground propagation models for UAV in mmWave bands. For this reason, we utilize the closest AP to UE propagation model by 3GPP.

Antenna directivity gain is given by $G = (4\pi R^2)/S_A$, where 4π is an area of the ideal isotropic radiator wavefront at the distance of R and S_G is the antenna wavefront area [17]. In our case, this is a spherical cap area, which implies that $S_G = 2\pi Rh$, where h can be derived from the antenna directivity angle as $h = R(1 - \cos[\alpha/2])$, see Fig. 2, where the model of the radiation pattern and the geometry of the model are illustrated. Assuming that all the radiation is now concentrated within the considered area, the antenna gain in question can be approximated by

$$A = \frac{4\pi}{S_G} = \frac{2}{1 - \cos[\alpha/2]}. \quad (1)$$

We introduce the coefficient $A = P_T GC$, where P_T is the transmit power, while the received power is $P = P_T GCr^{-\gamma} = Ar^{-\gamma}$. The LoS path between the mmWave AAP and the UE in urban environments can be blocked by (i) large stationary objects, such as buildings, and (ii) smaller moving objects, such as humans. According to 3GPP [16], the probability of blockage by the former is referred to as the non-LoS state of the channel. Here, we consider an open-space scenario typical for drones, where there are no buildings; thus, we address only the LoS state of the channel. We also disregard blockage by humans, since the relatively high altitudes of drones as compared to e.g., stationary APs make this component negligible.

III. Proposed 3D Modeling Approach

We concentrate on evaluating the SIR that is expressed as

$$S = \frac{P}{I} = \frac{Ad_0^{-\gamma}}{A\sum_{i=1}^{N} d_i^{-\gamma}} = \frac{d_0^{-\gamma}}{\sum_{i=1}^{N} d_i^{-\gamma}}, \quad (2)$$

where P is the received power, I is the aggregate interference power, N is a Poisson random variable (RV) with the mean of $\lambda\pi R_I^2$, d_0 is the $\Re^3$ distance between the communicating entities, and d_i, $i = 1, 2, \ldots, N$, are the $\Re^3$ distances corresponding to the interference paths to each interferer.

To obtain the mean SIR, we employ the Taylor series expansion of the SIR function, $S = g(x, y) = P(x)/I(y)$. The second-order approximation is obtained by expanding $g(x, y)$ around $\vec{\mu} = (E[P], E[I]) = (\mu_P, \mu_I)$ as

$$E[g(\vec{\mu})] \approx g(\vec{\mu}) + \frac{g''_{xx}(\vec{\mu})\sigma_P^2 + 2g''_{xy}K_{P,I} + g''_{yy}(\vec{\mu})\sigma_I^2}{2}, \quad (3)$$

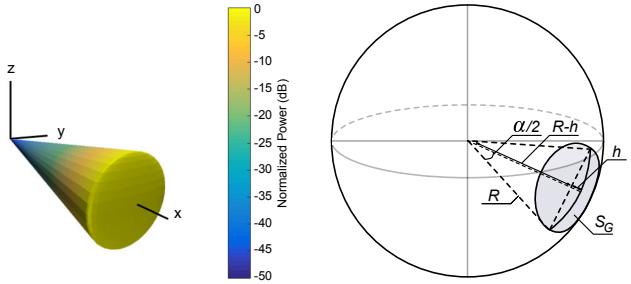

(a) Antenna model (b) Model geometry

Fig. 2. Illustration of antenna model and associated geometry.

where $K_{P,I}$ is the covariance between P and I, while σ_P^2 and σ_I^2 are the variances of P and I. Observing that $g''_{xx}(x,y)=0$, $g''_{x,y}(x,y)=-y^{-2}$, and $g''_{yy}(x,y)=2x/y^2$, we arrive at

$$E[P/I] \approx \mu_P/\mu_I - K_{P,I}/\mu_I^2 + \sigma_I^2\mu_P/\mu_I^3. \tag{4}$$

The moments of interference can be obtained as in [18],

$$E[I^n] = \int_S E\left[I_1^n(r)\right] p_C(r) dS, \tag{5}$$

where $dS = 2\lambda\pi r$ is the probability that there exists an interferer in the infinitesimal increment of the circumference, $p_C(r)$ is the probability that the transmit antenna at a drone acting as interferer and located at the planar distance of x from the tagged UE is oriented such that the interference power reaches the tagged UE, named here *directional exposure probability*, and $E\left[I_1^n(r)\right]$ are the moments of interference from a single transmitter at the distance of r.

Note that our proposed methodology can be employed to obtain other metrics of interest, including the signal-to-interference-plus-noise ratio (SINR), spectral efficiency, and Shannon capacity. The only modification needed is to expand the appropriate function into a Taylor series similarly to (3). To obtain the mean SIR, the following is required: (i) mean received signal strength, (ii) first two conditional moments of interference from a single AAP, (iii) directional exposure probability, and (iii) covariance between the received signal and interference. The propositions below establish these.

Proposition 1 (Mean Received Power)**.** *The moments of the received signal power are given by*

$$E[P^n] = A^n 2^{\frac{1}{2}-\gamma n}\left[W\left(\mu_T,\mu_R\right)+W\left(\mu_R,\mu_T\right)\right]\times \\ \times \frac{\pi^{\frac{3}{2}}\csc\left(\frac{\pi\gamma n}{2}\right)\sec\left(\frac{\pi\gamma n}{2}\right)R_T^{-\left(\frac{n\gamma-5}{2}\right)}}{\mu_R^2\mu_T^2\left(\mu_R+\mu_T\right)\Gamma\left(\frac{n\gamma}{2}\right)\Gamma\left(\frac{n\gamma-1}{2}\right)}, \tag{6}$$

where $W(x,y)$ is characterized as

$$W(x,y) = x^3\left[2\sqrt{2}y^{\gamma n}R_T^{\frac{n\gamma+1}{2}} + R_T^2 2^{\frac{\gamma n}{2}} y^{\frac{n\gamma+3}{2}}\Gamma\left(\frac{n\gamma-1}{2}\right)\times\right. \\ \left.\times\left(\cos\left(\frac{\pi\gamma n}{2}\right)H^{yR_T}_{\frac{3-n\gamma}{2}} - J^{yR_T}_{\frac{n\gamma-3}{2}} - \sin\left(\frac{\pi\gamma n}{2}\right)J^{yR_T}_{\frac{3-n\gamma}{2}}\right)\right],$$

where $\Gamma(z)$ is the Euler Gamma function, J_n^z is the Bessel function of the first kind, and H_n^z is the Struve function.

Proof. The power of the received signal can be expressed as $P = A\left(\sqrt{(H_T-H_R)^2+r^2}\right)^{-\gamma}$, where H_T, H_R, and r are the corresponding RVs. Since H_T and H_R follow the exponential distribution, the joint probability density function (jpdf) of $|H_T-H_R|$ is

$$f_{|H_T-H_R|}(y) = \frac{(e^{-y\mu_R}+e^{-y\mu_T})\mu_R\mu_T}{\mu_R+\mu_T},\ y>0. \tag{7}$$

Based on [19], the moments $E[P^n(r)]$, $n=1,2,\ldots$, of the received signal power can be expressed as

$$E[P^n] = \int_0^{R_T}\int_0^{\infty} \frac{A^n\left(e^{-y\mu_R}+e^{-y\mu_T}\right)\mu_R\mu_T 2r}{\left(r^2+y^2\right)^{\frac{n\gamma}{2}}\left(\mu_R+\mu_T\right)R_T^2} dydr. \tag{8}$$

Evaluating the integrals in (8), we arrive at (9). □

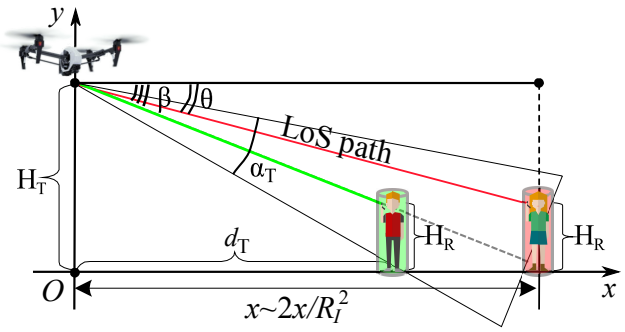

Fig. 3. An illustration of interference in three dimensions.

Corollary 1 (Conditional Moments of Interfering Signal from a Single AAP)**.** *The conditional moments of interference are obtained by fixing the distance between the AAP and the UE on the ground as*

$$E[I_1^n(r)] = \frac{\left[\left(\mu_R+\mu_T\right)\Gamma\left(\frac{n\gamma}{2}\right)\right]\left[W_1(\mu_T)+W_1(\mu_R)\right]}{2^{-\frac{n\gamma+1}{2}}A^n\pi^{\frac{3}{2}}\mu_R\mu_T}, \tag{9}$$

where $1(x)$ is given by

$$W_1(x) = \left[\frac{r}{x}\right]^{\frac{1-n\gamma}{2}}\left[2J^{rx}_{\frac{n\gamma-1}{2}}\csc\left(n\pi\gamma\right) - \right. \\ \left. - J^{rx}_{\frac{1-n\gamma}{2}}\sec\left(\frac{n\pi\gamma}{2}\right) + \csc\left(\frac{n\pi\gamma}{2}\right)H^{rx}_{\frac{1-n\gamma}{2}}\right]. \tag{10}$$

The directional exposure probability $p_C(r)$ can be approximated by $p_C(r) = p_V(r)p_H(r)$, where $p_H(r)$ is the probability that the interferer exposes the tagged UE in two dimensions, $p_V(r)$ is the probability that this also occurs in the third ('vertical') dimension. The two-dimensional exposure probability, p_H, is $p_H(r) = \alpha r/2\pi r = \alpha/2\pi$.

Proposition 2 ('Vertical' Exposure Probability)**.** *The 'vertical' exposure probability, $p_V(r)$, is established by integrating the jpdf of angles β and θ over $|\beta-\theta|<\alpha/2$ (see Fig. 3), that is,*

$$p_V(r) = \int_{-\frac{\pi}{2}}^{\frac{\pi}{2}}\int_{y_4-\frac{\alpha}{2}}^{y_4+\frac{\alpha}{2}} W_{\beta,\theta}\left(y_1,y_4\right)dy_1dy_4, \tag{12}$$

where $W_{\beta,\theta}\left(y_1,y_4\right)$ is the jpdf of β and θ in the form of (11).

Proof. Let $\xi_1^n = \{\xi_1,\xi_2,\ldots,\xi_4\} = \{H_R,H_T,d_T,H_I\}$. Observe that the jpdf of these RVs has a multiplicative form due to their independence, which yields

$$\omega_{\xi_1^n}\left(r_1^n\right) = \mu_R e^{-\mu_R x_1}\mu_T e^{-\mu_T x_2}2x_3\mu_R e^{-\mu_R x_4}/R_T^2. \tag{13}$$

Relabeling the target RVs as $\eta_1^m = \{\eta_1,\eta_4\} = \{\beta,\theta\}$, we note that $m<n$. Complementing the set of target RVs as

$$\eta_1^n = \{\eta_1,\eta_2,\ldots,\eta_4\} = \{\beta,H_T,d_T,\theta\}, \tag{14}$$

we define the transformation as

$$\begin{cases} y_1 = \tan^{-1}\ \left([x_1-x_2]/x_3\right) = \beta, \\ y_2 = x_2, \\ y_3 = x_3, \\ y_4 = \tan^{-1}\ \left([x_4-x_2]/r\right) = \theta. \end{cases} \tag{15}$$

$$W_{\beta,\theta}\left(y_1,y_4\right)=\begin{cases}\frac{-2r\mu_T\cot(y_1)\csc^2(y_1)\sec^2(y_4)}{R_T^2\mu_R(2\mu_R+\mu_T)}\mathrm{e}^{-\mu_R(R_T\tan(y_1)+r\tan(y_4))}\times & \\ \times\left(2-2\mathrm{e}^{R_T\mu_R\tan(y_1)}+2R_T\mu_R\tan(y_1)+R_T^2\mu_R^2\tan^2(y_1)\right) & y_1\geq 0\wedge y_4\geq 0\\ \frac{2r\mu_T\cot(y_1)\csc^2(y_1)\sec^2(y_4)}{R_T^2\mu_R(2\mu_R+\mu_T)}\mathrm{e}^{-R_T\mu_R\tan(y_1)+r(\mu_R+\mu_T)\tan(y_4)}\times & (y_1\geq 0\wedge y_4<0)\vee\\ \times\left(-2+2\mathrm{e}^{R_T\mu_R\tan(y_1)}-2R_T\mu_R\tan(y_1)-R_T^2\mu_R^2\tan^2(y_1)\right) & (y_4<0\wedge R_T\tan(y_1)\geq r\tan(y_4))\\ \frac{2\mathrm{e}^{-r\mu_R\tan(y_4)}r\mu_R^2\mu_T\cot(y_1)\csc^2(y_1)\sec^2(y_4)}{R_T^2(\mu_R+\mu_T)^3(2\mu_R+\mu_T)}\times & \\ \times\left(\begin{array}{l}-2+\mathrm{e}^{R_T(\mu_R+\mu_T)\tan(y_1)}\times\\ \times\left(2+R_T(\mu_R+\mu_T)\tan(y_1)\left(-2+R_T(\mu_R+\mu_T)\tan(y_1)\right)\right)\end{array}\right) & y_1<0\wedge y_4\geq 0\\ \frac{-2\mathrm{e}^{-r\mu_R\tan(y_4)}r\mu_T\cot(y_1)\sec^2(y_4)}{R_T^2\mu_R(\mu_R+\mu_T)^3(2\mu_R+\mu_T)}\times & \\ \times\left(\begin{array}{l}2\mathrm{e}^{R_T(\mu_R+\mu_T)\tan(y_1)}R_T\mu_R^3(\mu_R+\mu_T)\csc(y_1)\sec(y_1)-\\ -\mathrm{e}^{R_T(\mu_R+\mu_T)\tan(y_1)}R_T^2\mu_R^3(\mu_R+\mu_T)^2\sec^2(y_1)+\csc^2(y_1)\times\\ \times\left(\begin{array}{l}2\left(\begin{array}{l}-\mathrm{e}^{R_T(\mu_R+\mu_T)\tan(y_1)}\mu_R^3-\mathrm{e}^{r(2\mu_R+\mu_T)\tan(y_4)}(\mu_R+\mu_T)^3+\\ +\mathrm{e}^{r(\mu_R+\mu_T)\tan(y_4)}(2\mu_R+\mu_T)\left(\mu_R^2+\mu_R\mu_T+\mu_T^2\right)\end{array}\right)+\\ +\mathrm{e}^{r(\mu_R+\mu_T)\tan(y_4)}r\mu_R(\mu_R+\mu_T)(2\mu_R+\mu_T)\tan(y_4)\times\\ \times\left(2\mu_T+r\mu_R(\mu_R+\mu_T)\tan(y_4)\right)\end{array}\right)\end{array}\right) & \text{elsewhere}\end{cases}\tag{11}$$

The inverse transform is a one-to-one mapping in the domains of β and $\theta=(-\pi/2,\pi/2)$ (bijection). Therefore,

$$\begin{cases}x_1=\varphi_1\left(y_1^n\right)=y_2+y_3\tan y_1,\\ x_2=\varphi_2\left(y_1^n\right)=y_2,\\ x_3=\varphi_3\left(y_1^n\right)=y_3,\\ x_4=\varphi_4\left(y_1^n\right)=y_2+r\tan y_4.\end{cases}\tag{16}$$

The sought jpdf is then given by

$$W_{\eta_1^n}\left(y_1^n\right)=\omega_{\xi_1^n}\left[\varphi_1\left(y_1^n\right),\ldots,\varphi_n\left(y_1^n\right)\right]|J|,\tag{17}$$

where the Jacobian is computed as $J=y_3rsec^2y_1sec^2y_4$, while $\omega_{\xi_1^n}\left[\varphi_1\left(y_1^n\right),\ldots,\varphi_n\left(y_1^n\right)\right]$ can be produced as

$$\frac{2\mathrm{e}^{-y_2\mu_T-\mu_R(y_2+y_3\tan[y_1])-\mu_R(y_2+r\tan[y_4])}y_3\mu_R^2\mu_T}{R_T^2}.\tag{18}$$

Evaluating the subject integrals leads to

$$W_{\eta_1,\eta_4}\left(y_1,y_4\right)=\iint\limits_{\Re^2}\frac{\omega_{(\xi_1^n)}\left[\varphi_1\left(y_1^n\right),\ldots,\varphi_n\left(y_1^n\right)\right]}{|J|^{-1}}dy_2dy_3=$$

$$=\int\limits_0^{R_T}\int\limits_{m(y_1,y_4)}^{\infty}\frac{2y_3\mu_R^2\mu_Try_3\sec^2\left(y_1\right)\sec^2\left(y_4\right)dy_2dy_3}{R_T^2e^{y_2\mu_T+\mu_R(y_2+y_3\tan(y_1))+\mu_R(y_2+r\tan(y_4))}}=$$

$$=\int\limits_0^{R_T}\frac{2ry_3^2\mu_R^2\mu_T\sec^2\left(y_1\right)\sec^2\left(y_4\right)\left(2\mu_R+\mu_T\right)^{-1}dy_3}{e^{(2\mu_R+\mu_T)m(y_1,y_4)+\mu_R(y_3\tan(y_1)+r\tan(y_4))}},\tag{19}$$

where $m(y_1,y_4)=\max\left\{0,-y_3\tan\left(y_1\right),-x\tan\left(y_4\right)\right\}$. Considering the last integral, we obtain the jpdf $W_{\eta_1,\eta_4}\left(y_1,y_4\right)$ in its closed form (11). □

Proposition 3 (Covariance $K_{P,I}$)**.** *The covariance between the interference and the received signal may be determined as*

$$K_{P,I}=A^2\lambda\pi R_I^2p_CE[(X_iX_0)^{-\gamma}]-\mu_P\mu_I,\tag{20}$$

where $E[(X_0X_i)^{-\gamma}]$ is obtained by numerical integration,

$$\int\limits_0^{R_I}\int\limits_0^{R_T}\int\limits_0^{\infty}\int\limits_0^{\infty}\int\limits_0^{\infty}\frac{\left[(x_1-x_2)^2+x_5^2\right]^{-\frac{\gamma}{2}}}{\left[(x_1-x_3)^2+x_4^2\right]^{\frac{\gamma}{2}}}f(x_1,..,x_5)dx_1..dx_5,\tag{21}$$

with the associated jpdf provided in the following form

$$f(x_1,\ldots,x_5)=\frac{\mu_T\mu_R^2e^{-\mu_Tx_1-\mu_R(x_2+x_3)}4x_4x_5}{(R_TR_I)^2}.\tag{22}$$

Proof. Rewrite $K_{P,I}$ as $K_{P,I}=E[PI]-\mu_P\mu_I$, where μ_P and μ_I have been established previously. Next, the Wald's identity [19] is applied to $E[PI]$ as

$$\begin{aligned}K_{P,I}&=E[PI]-\mu_P\mu_I=\\&=E\Big[AX_0^{-\gamma}\sum_{i=1}^{N}AX_i^{-\gamma}\Big]-\mu_P\mu_I=\\&=A^2\lambda\pi R_I^2p_CE[(X_iX_0)^{-\gamma}]-\mu_P\mu_I,\end{aligned}\tag{23}$$

where X_0 is the distance between the AAP and the UE of interest, X_i, $i=1,2,\ldots,N$, are the distances between the interferers and the said UE, and N is the number of interferers; $E[N]=\lambda\pi R_I^2p_C$ and $E[(X_0X_i)^{\gamma}]$ are the only unknowns. Note that here we apply the Wald's identity [19] and thus can rewrite $E[(X_0X_i)^{-\gamma}]$ by using the random heights as

$$E\Big[\Big(\left[(H_R-H_T)^2-r_0\right]\left[(H_R-H_I)^2-r_i\right]\Big)^{-\frac{\gamma}{2}}\Big],\tag{24}$$

where r_0 is a constant; we thus arrive at (20). □

The complexity of the numerical integration in (21) depends on the integration order. By choosing it as shown in (21), only two latter integrals needs to be evaluated numerically.

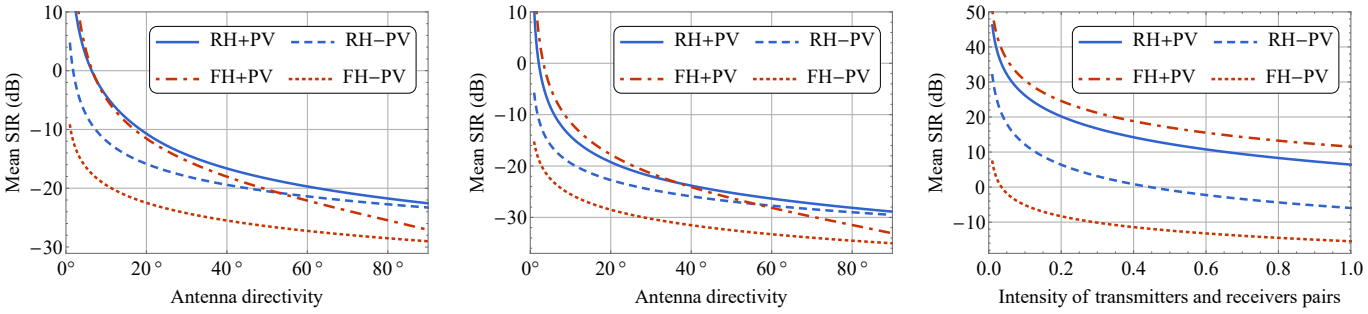

(a) $\lambda = 0.5$ (b) $\lambda = 2.0$ (c) $\alpha = 2°$

Fig. 4. Mean SIR as a function of antenna directivity α and intensity of AAP–UE pairs λ.

IV. Numerical Analysis

Our developed 3D model is rather complex as it involves numerical integration of (11) according to (12) and in (21). Assuming fixed heights of both the AAPs and the UEs, the solution becomes much simpler since the joint distribution of β and θ depends only on one RV. Further, disregarding the heights of AAPs and UEs leads to a two-dimensional formulation, where the expressions for the moments of SIR are available in the closed form [15]. A natural research question is then "can we still apply simpler (e.g., 2D) models to accurately represent SNR?"

Below, we first assess the accuracy of our proposed model and then conduct a numerical study on the discrepancy that arises as a result of replacing the true 3D model with its simplifications. We concentrate on the carrier frequency of 28 GHz. The propagation coefficients C and γ that correspond to this frequency are computed to be 28935037 and 2.1, respectively. The maximum association distance of R_T is 15 m, while the interference radius is calculated dynamically, since it is affected by the antenna directivity angle α.

A. Accuracy of models

We first assess the accuracy of our developed 3D model and its simplified formulation by comparing the corresponding results with simulations. Fig. 5 illustrates the mean SIR as a function of antenna directivity α for the intensity of AAP arrival process $\lambda = 0.5$, where RH and FH represent the random and fixed heights of AAPs and UEs, respectively, PV is the 'vertical' exposure probability, while sign '+' implies that p_V is taken into account. The mean heights of the AAPs and the UEs are set to $E[H_T] = 40$ m and $E[H_R] = 1.7$ m. Our simulation results are displayed by using ticks of the same color. Both the proposed 3D model as well as its simplified version agree well with the simulations. Similar observations can be made for different intensities λ and various mean heights $E[H_T]$ and $E[H_R]$.

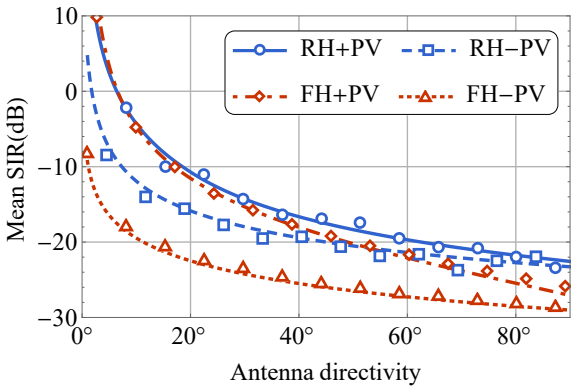

Fig. 5. Accuracy assessment of our developed model.

B. Comparison of models

The mean SIR as a function of the antenna directivity angle α and the intensity of AAP arrivals λ is illustrated in Fig. 4 for $E[H_T] = 40$ m and $E[H_R] = 1.7$ m. First, we note that for the considered models the mean SIR decreases as α grows, thus implying that they correctly capture the qualitative system behavior. However, the quantitative difference between these results is due to the 'vertical' exposure probability p_V; it increases as α becomes smaller. Particularly, the model with fixed heights and without considering the 'vertical' exposure probability for $\lambda = 0.5$ underestimates the mean SIR by approximately 7 dB for $\alpha = 60°$ and by 27 dB for $\alpha = 2°$. Similar figures are observed for $\lambda = 2$. The model with random heights that does not take into account the 'vertical' exposure probability converges to the formulation with the 'vertical' exposure probability accounted for as α grows.

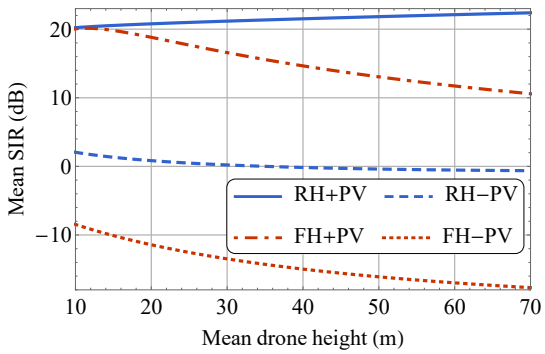

Fig. 6. Effect of AAP height on mean SIR.

The closest approximation with regards to our developed model is given by the approach that takes p_V into account and has fixed heights of AAPs and UEs. However, this

approximation depends on the antenna directivity angle. For smaller values of α, the model with fixed heights overestimates the actual mean SIR. After increasing α, the model begins to underestimate the mean SIR, and the gap may reach several decibels for $\alpha > 80°$. In this regime, the use of the model with random heights that disregards the 'vertical' exposure probability is more appropriate. The results presented in Fig. 4(c) indicate that the value of λ does not affect the discrepancy between the models drastically, since the distance between the curves is preserved across the entire range of the considered intensities.

The effect of the mean height of the AAPs on the average SIR for $\alpha = 2°$, $\lambda = 0.5$, and $E[H_R] = 1.7$ m is displayed in Fig. 6. The model that neglects the 'vertical' exposure probability drastically underestimates the mean SIR for all the considered values of $E[H_T]$. Furthermore, significant underestimation is observed for the model with fixed heights and 'vertical' exposure probability at $E[H_T] > 20$.

V. Conclusions

In this paper, we developed a 3D model for drone-based mmWave communication that explicitly takes into account the random heights of drone-transceivers, or AAPs, and the UEs as well as the 'vertical' exposure probability. Our simulations confirmed the accuracy of the proposed model. The subsequent numerical analysis demonstrated that capturing the 'vertical' exposure probability as well as the random heights of AAPs and UEs to assess the aggregate interference is of crucial importance. The simpler models are not capable of providing accurate approximations of the mean SIR across the entire feasible range of input parameters.

For the specific ranges of antenna directivity values α, one can however resort to such simpler formulations. Particularly, when $\alpha > 60°$ the model without the 'vertical' exposure probability delivers an adequate approximation for the considered AAP arrival intensities. When $\alpha < 10°$, the model with the 'vertical' exposure probability as well as the fixed heights of AAPs and UEs that are equal to their mean values becomes sufficiently accurate.

Acknowledgments

The publication was supported by the Ministry of Education and Science of the Russian Federation (project No. 2.3397.2017/4.6).

References

[1] Y. Zeng, R. Zhang, and T. J. Lim, "Wireless communications with unmanned aerial vehicles: opportunities and challenges," *IEEE Comm. Mag.*, vol. 54, no. 5, pp. 36–42, 2016.

[2] J. Li, G. Deng, C. Luo, Q. Lin, Q. Yan, and Z. Ming, "A Hybrid Path Planning Method in Unmanned Air/Ground Vehicle (UAV/UGV) Cooperative Systems," *IEEE Trans. on Veh. Tech.*, vol. 65, no. 12, pp. 9585–9596, 2016.

[3] M. Chen, M. Mozzaffari, W. Saad, C. Yin, M. Debbah, and C. Hong, "Caching in the Sky: Proactive Deployment of Cache-Enabled Unmanned Aerial Vehicles for Optimized Quality-of-Experience," *IEEE J. on Sel. Ar. on Comm.*, vol. 35, no. 6, pp. 1046–1061, 2017.

[4] M. DeGrasse, "AT&T explains drone trials," https://www.rcrwireless.com/20160714/network-infrastructure/att-launches-drone-trials-tag4, RCRWirelessNews, Tech. Rep., 2016.

[5] A. Orsino, A. Ometov, G. Fodor, D. Moltchanov, L. Militano, S. Andreev, O. N. Yilmaz, T. Tirronen, J. Torsner, G. Araniti *et al.*, "Effects of heterogeneous mobility on D2D- and drone-assisted mission-critical MTC in 5G," *IEEE Comm. Mag.*, vol. 55, no. 2, pp. 79–87, 2017.

[6] Y. Zeng, R. Zhang, and T. J. Lim, "Throughput maximization for UAV-enabled mobile relaying systems," *IEEE Trans. on Comm.*, vol. 64, no. 12, pp. 4983–4996, 2016.

[7] A. Fotouhi, M. Ding, and M. Hassan, "DroneCells: Improving 5G Spectral Efficiency using Drone-mounted Flying Base Stations," *arXiv:1707.02041*, 2017.

[8] I. Bor-Yaliniz and H. Yanikomeroglu, "The new frontier in ran heterogeneity: Multi-tier drone-cells," *IEEE Comm. Mag.*, vol. 54, no. 11, pp. 48–55, 2016.

[9] V. Sharma, M. Bennis, and R. Kumar, "UAV-assisted heterogeneous networks for capacity enhancement," *IEEE Comm. Lett.*, vol. 20, no. 6, pp. 1207–1210, 2016.

[10] M. Mozaffari, W. Saad, M. Bennis, and M. Debbah, "Unmanned aerial vehicle with underlaid device-to-device communications: Performance and tradeoffs," *IEEE Trans. on Wirel. Comm.*, vol. 15, no. 6, pp. 3949–3963, 2016.

[11] M. Mozaffari, W. Saad, M. Bennis, and M. Debbah, "Efficient deployment of multiple unmanned aerial vehicles for optimal wireless coverage," *IEEE Comm. Lett.*, vol. 20, no. 8, pp. 1647–1650, 2016.

[12] A. Samuylov, M. Gapeyenko, D. Moltchanov, M. Gerasimenko, S. Singh, N. Himayat, S. Andreev, and Y. Koucheryavy, "Characterizing spatial correlation of blockage statistics in urban mmWave systems," in *Proc. of GC Wkshps*. IEEE, 2016, pp. 1–7.

[13] V. Petrov, D. Solomitckii, A. Samuylov, M. A. Lema, M. Gapeyenko, D. Moltchanov, S. Andreev, V. Naumov, K. Samouylov, M. Dohler *et al.*, "Dynamic multi-connectivity performance in ultra-dense urban mmWave deployments," *IEEE J. on Sel. Ar. in Comm.*, vol. 35, no. 9, pp. 2038–2055, 2017.

[14] Z. Xiao, P. Xia, and X.-G. Xia, "Enabling UAV cellular with millimeter-wave communication: Potentials and approaches," *IEEE Comm. Mag.*, vol. 54, no. 5, pp. 66–73, 2016.

[15] V. Petrov, M. Komarov, D. Moltchanov, J. M. Jornet, and Y. Koucheryavy, "Interference and SINR in Millimeter Wave and Terahertz Communication Systems With Blocking and Directional Antennas," *IEEE Trans. on Wirel. Comm.*, vol. 16, no. 3, pp. 1791–1808, 2017.

[16] 3GPP, "Study on channel model for frequencies from 0.5 to 100 GHz (Release 14)," 3GPP TR 38.901 V14.1.1, July 2017.

[17] T. S. Rappaport *et al.*, *Wireless communications: principles and practice*. Prentice hall PTR New Jersey, 1996, vol. 2.

[18] S. Chiu, D. Stoyan, W. Kendall, and J. Mecke, *Stochastic geometry and its applications*. Wiley, 2013.

[19] S. Ross, *Introduction to probability models*. Academic Press, 2010.